

# A GIC-Inclusive State Estimator for Power System Awareness during Geomagnetic Disturbance Events

Gandhali Prakash Juvekar, *Student Member, IEEE*, Cecilia Klauber, *Student Member, IEEE*,  
Katherine Davis, *Senior Member, IEEE* Thomas J. Overbye, *Fellow, IEEE*  
and Komal Shetye, *Senior Member, IEEE*

**Abstract**—Geomagnetic disturbances (GMDs) threaten the secure and reliable operation of the electric power grid. During a GMD, geomagnetically induced currents (GICs) cause additional reactive power losses and a lowered voltage profile. Preventing and mitigating a widespread system collapse in such an occurrence requires accurate knowledge of the current system state. This is provided by power system state estimation, but as traditional methods do not account for GIC-related monitoring and modeling, they may fail to provide accurate results during a GMD. Therefore, in this work excess reactive power losses are explicitly modeled in the state estimation method and GIC-related values are included among the states and measurements. The modeling scheme is thoroughly discussed and estimation results on a 20 bus and 150 bus case validate the estimation accuracy improvement provided by a GIC-inclusive modified state estimator during a GMD.

**Index Terms**—Geomagnetic disturbance (GMD), geomagnetically induced currents (GICs), state estimation, modeling, reactive power losses.

## I. INTRODUCTION

POWER systems are critical infrastructures required for delivery of electric power. While this system is robust, challenges exist that disrupt operations. The disturbances can be localized or regional and can be natural or man-made. A geomagnetic disturbance (GMD) is a natural force that has the potential to disrupt the operations of the power grid. In a GMD, coronal mass ejections discharging from the sun's surface disturb the earth's magnetic field, causing it to vary rapidly [1], [2]. Following Faraday's law of electromagnetic induction, a varying magnetic field produces an electric field over the earth's surface in the region affected. This electric field in turn induces a surface potential along long-distance, high-voltage transmission lines. This voltage drives geomagnetically induced currents (GICs) to flow through the lines, neutral-grounded transformers and the ground, forming a circuit. When these quasi-dc (less than 1 Hz) GICs flow through high-power transformers, they can cause half cycle saturation which results in reactive power losses. This can also cause transformer heating and damage. GICs produce harmonics in the system which can trip control and protection devices. The

This work is funded by National Science Foundation through "EAR-1520864: Hazards SEES: Improved prediction of geomagnetic disturbances, geomagnetically induced currents, and their impacts on power distribution systems".

The authors are with the Dept. of ECE, Texas A&M University, College Station, TX, USA;  
Emails: gandhalijuvekar, cklauber, katedavis, overbye, shetye@tamu.edu

tripping of reactive power support in the system can disturb the voltage profile across the system. If these problems persist, it can eventually lead to voltage collapse [3]. The GMD event of 1989 that occurred in the Hydro-Quebec region caused a blackout that lasted nine hours. Multiple transformers were damaged, and their cascading failures led to a total voltage collapse [4], [5]. Hence, a GMD has the potential to cause long-term damage to the grid, leave people without power for extended periods of time, and negatively impact emergency services and public safety.

The grid needs to be resilient to such GMD hazards, and this can be possible with real-time monitoring and event analysis as well as by preparing response action plans. The North American Electric Reliability Corporation (NERC) first mandated assessments and plans to address the impacts of GMD for the industry in 2014 [6], [7]. Various efforts have been pursued including mitigation techniques, voltage analysis, reliability assessment, improved GIC modeling, and GIC monitoring to list a few [8]–[13].

One less explored aspect of addressing GMD effects is to look at these events from a power system state estimation (PSSE) perspective. Briefly put, the state of the system can be estimated using an accurate power flow model and available measurements [14]–[16]. While extensions in this well-researched area include improved methods during abnormal conditions, such as cyber-attack and other extreme situations [17]–[20], the extent of specialized applications of PSSE during a GMD is to estimate just the underlying geoelectric field, not the full system state [21]. Previous work has shown that the traditional PSSE model falls short in providing the accurate system states during a GMD event [22]. Traditional estimators incur additional error from the lack of GMD modeling, and the resulting estimates may induce unreliable results if used in additional tools, applications, or algorithms. The operational ramifications of such erroneous inputs include misoperation and making the situation worse, not better. Therefore, a modified or GIC-inclusive state estimator can immensely aid system operators. The more accurate states obtained using this state estimator can help operators decide on the correct steps to take to curb the ill-effects of the event.

To address these needs, this paper contributes an algorithm for GIC-inclusive PSSE for GMD events. GIC-related measurements, namely neutral current measurements and electric field-based pseudomeasurements, are leveraged and GIC-induced reactive power losses are explicitly included in the state estimation model. The algorithm is implemented in MAT-

LAB upon the MATPOWER state estimation package [23]. Measurements are obtained from a power flow software and additive noise is added to mimic real-life measurements. The measurement set includes traditional state estimator measurements along with measurements from transformer neutral GIC monitoring devices and pseudomeasurements derived from electric field information. The states comprise of the traditional states (voltage magnitude and angle) along with the system transformer neutral currents. The estimator is tested on two systems under varying GMD scenarios: a 20 bus case [24] and a 150 bus case [25]. The resulting error profiles are plotted and compared with the results of a traditional state estimator. [A bad data detection method for the proposed estimator is also developed and tested.](#)

The paper is organized as follows: the dc GIC model and the resulting ac effects are introduced in Section II. The traditional estimation methods and its shortcomings are discussed in Section III. The formulation and implementation of the proposed estimator is described in Section IV. In Section V, the results are presented and discussed. The conclusion and future work are detailed in Section VI.

## II. GIC MODELING

### A. DC Modeling

GICs circulating in the system depend on the electric field over the region affected by the GMD, as well as the dc parameters and topology of the system [26]–[28]. The voltages induced in the transmission lines by the geoelectric field are quasi-dc in nature and hence, the GICs are modeled via the dc network analysis [29] given by:

$$\mathbf{I} = \mathbf{G}\mathbf{V} \quad (1)$$

where  $\mathbf{G}$  is the dc conductance matrix of the system including values for substation nodes.  $\mathbf{V}$  is the vector comprised of the bus and substation dc voltages. The vector  $\mathbf{I}$  consists of injection currents at every node in the system - bus and substation. The injection current at every node depends linearly on the electric field  $\mathbf{E}$  and the direction and length of the transmission lines. The GIC flowing from node  $n$  to node  $m$  in the network is given by the equation,

$$I_{nm} = g_{nm}(V_n - V_m) \quad (2)$$

where  $g_{mn}$  is the dc conductance of the connecting line/transformer.

Let the quasi-dc effective per phase GIC current for transformer  $t$  be  $\mathcal{I}_t$ .  $\mathcal{I}_t$  is the current flowing through the high-side winding for delta-wye transformers.  $\mathcal{I}_t$  is a combination of the currents flowing through both high-side and low-side coils for autotransformers and wye-wye transformers. According to [30], the equation for effective GICs is given by

$$\mathcal{I}_t = \left| I_{H,t} + \frac{I_{L,t}}{a_t} \right| \quad (3)$$

where the per phase GIC flowing through the high side transformer coil is  $I_{H,t}$ , the per phase GIC flowing through the low side transformer coil is  $I_{L,t}$ , and the transformer turns ratio is  $a_t$ .  $I_{H,t}$  and  $I_{L,t}$  can be obtained using Eq. 2.

### B. AC Modeling of GIC Effects

GMDs affect transformers in the system, where higher magnetizing currents from core saturation lead to additional reactive power losses. Using the fundamental frequency component, these losses are modeled as linearly dependent on transformer effective GICs [31], [32] and expressed by

$$Q_{loss,t} = k_t V_{pu,t} \mathcal{I}_t \quad (4)$$

where the ac voltage (pu) at the transformer high side bus is  $V_{pu,t}$ , and  $k_t$  (MVar/A) is a transformer-dependent scalar which may be nonlinear but is acceptably modeled as linear in Eq. 4 [33], [34]. This reactive power loss is not accounted for in the traditional state estimation measurement model, outlined in Section III. The contribution of this work is amending existing formulations to incorporate this relevant value.

## III. TRADITIONAL STATE ESTIMATION

Supervisory Control and Data Acquisition (SCADA) and increasingly available metering make real-time monitoring of the system possible. Situational awareness obtained from the system states enables effective management of the system [15], [16]. A typical PSSE algorithm is formulated as solving an over-determined system for a non-linear ac power flow. The non-linear system equations are often solved using the weighted least square (WLS) approach [16]. Let the system states be indicated by  $\mathbf{x}$  which is a vector of length  $n$ . The states are typically bus voltage angles and magnitudes. Let the measurements obtained from the system be indicated by  $\mathbf{z}$  which is a vector of length  $m$ . The measurement set typically consists of real and reactive power flows and injections, angle differences, voltage magnitudes, current flows and injections, turns ratios and transformer phase shift angles, if available. The model that relates the system states to the measurement  $i$  is given by

$$z_i = h_i(\mathbf{x}) + e_i \quad (5)$$

where the states  $\mathbf{x}$  are related to each measurement  $z_i$  through the non-linear function  $h_i(\cdot)$  and  $e_i$  is the measurement error and is assumed to have zero mean and variance  $\sigma_i^2$ .

The PSSE problem is formulated as a minimization optimization problem. For the WLS method, the standard solution approach involves iterative methods. For practical implementations, the Gauss Newton method is used. Let

$$\mathbf{J}(\mathbf{x}) = \frac{1}{2} \sum_{i=1}^m \frac{r_i^2}{\sigma_i^2} \quad (6)$$

where the residual  $r_i$  is  $z_i - h_i(\mathbf{x})$ . The Jacobian matrix  $\mathbf{H}$ , the diagonal weight matrix of measurement variances  $\mathbf{R}$ , and the residual  $\mathbf{r}$  are related by first-order optimality conditions. By Taylor series expansion and ignoring second-order terms, subsequent iterations can be calculated by

$$\Delta \mathbf{x}^k = \mathbf{G}(\mathbf{x}^k)^{-1} \mathbf{H}^T(\mathbf{x}^k) \mathbf{R}^{-1} \mathbf{r}(\mathbf{x}) \quad (7)$$

$$\mathbf{x}^{k+1} = \mathbf{x}^k + \Delta \mathbf{x}^k, \quad (8)$$

where  $\mathbf{G} = \mathbf{H}^T \mathbf{R}^{-1} \mathbf{H}$  is the gain matrix.

Ill-conditioning and convergence issues might occur because of non-linearity of the problem and weighting factor differences. The system also needs to be modeled accurately to avoid estimation errors and issues. Fig. 1 shows the number of trials out of 100 that converged using a traditional state estimator on a 150 bus case. An electric field was applied to the case with magnitude 4 V/km and direction varying from 0 to 360°. This shows how lack of proper modeling of GMD effects can lead to lack of situational awareness during a GMD. The following section details how traditional state estimation methods can be augmented to account for GMDs.

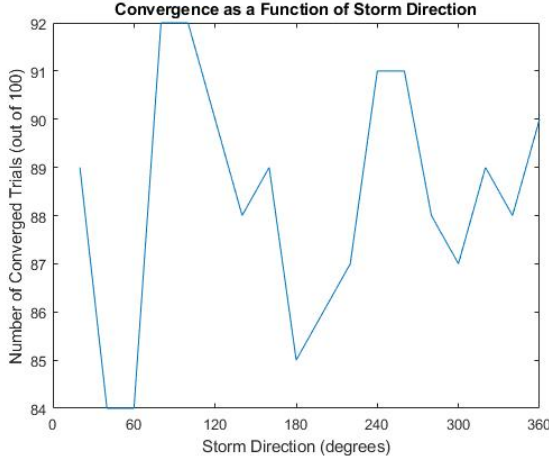


Fig. 1. Number of convergent trials (out of 100) using traditional state estimation methods with an electric field applied

#### IV. GIC-INCLUSIVE ESTIMATION FORMULATION

To formulate the GIC-inclusive estimator, the system models for power flows, injections, and line losses need to be updated to include the reactive power losses depicted in Eq. 4. These changes incur further updates to the elements of the classic solution method, namely the resulting components of the Jacobian matrix. The state and measurement vectors are extended to accommodate these updates. In this section, these changes and the corresponding derivation of terms are described in full. Additionally, a bad data detection method for the GIC-inclusive estimator is outlined.

##### A. Augmentation of State and Measurement Vectors

With the addition of GIC-inclusive models, GIC-related values are also added to the state and measurement vectors,  $\mathbf{x}$  and  $\mathbf{z}$ . Though the reactive power losses are directly dependent on effective GICs, transformer neutral GICs across the system are chosen to be the additional states, per-unitized for numerical purposes. Therefore, the augmented state vector is  $\mathbf{x} = [\boldsymbol{\theta}, \mathbf{V}_{pu}, \mathbf{I}_{n,pu}]^T$  where  $\boldsymbol{\theta}$  is the set of all bus voltage angles,  $\mathbf{V}_{pu}$  is the set of all bus voltage magnitudes (pu), and  $\mathbf{I}_{n,pu}$  is the set of all transformer neutral GICs (pu). Effective GICs are not directly measurable, but some systems do have the capability to measure select transformer neutral currents. Therefore, available GIC neutral measurements are added to the measurement vector, represented by

$\mathbf{z} = [\mathbf{P}_f, \mathbf{P}_{inj}, \boldsymbol{\theta}_{meas}, \mathbf{Q}_f, \mathbf{Q}_{inj}, \mathbf{V}_{meas}, \mathbf{I}_{n,meas}]^T$  where the sets of measured real and reactive power flows are  $\mathbf{P}_f$  and  $\mathbf{Q}_f$ , respectively, the sets of measured real and reactive power injections are  $\mathbf{P}_{inj}$  and  $\mathbf{Q}_{inj}$ , respectively, the set of measured voltage angles is  $\boldsymbol{\theta}_{meas}$ , the set of measured voltage magnitudes is  $\mathbf{V}_{meas}$ , and the set of measured transformer neutral GICs in pu is  $\mathbf{I}_{n,meas}$ . As electric field information is becoming increasingly available via measurement and estimation [35], [36], electric field input is not leveraged directly in the measurement vector, but indirectly through initialization and model parameters. Through intermediary means such as [37] this electric field information provides neutral GIC state guesses as well as modeling values for every iteration.

##### B. Updates to the Power Flow and Injection Models

The additional transformer reactive power loss due to GMD effects is represented by  $Q_{loss,i}$  because it is modeled at the high side bus,  $i$ . In conjunction with Eq. 4, an improved model for the reactive power injection at bus  $i$  ( $Q_{inj,i,new}$ ) is given by

$$Q_{inj,i,new} = Q_{inj,i,initial} + Q_{loss,i}$$

$$Q_{inj,i,new} = Q_{inj,i,initial} + V_{pu,i} \times \sum_{k=1}^{n_x} (k_{pu,tr_k} \times I_{eff,pu,tr_k}) \quad (9)$$

where  $Q_{inj,i,initial}$  represents the traditional reactive power model, from the classic power flow equations. Here,  $n_x$  refers to the number of adjacent lines with a transformer connected with the high side connected to the bus  $i$  and the subscript  $tr_k$  refers to the ' $k^{th}$ ' transformer. Similarly, the improved model for the reactive power flow from bus  $i$  to  $j$  ( $Q_{f,ij,new}$ ) is given by

$$Q_{f,ij,new} = Q_{f,ij,initial} + Q_{loss,ij}$$

$$Q_{f,ij,new} = Q_{f,ij,initial} + V_{pu,i} \times k_{pu,tr_k} \times I_{eff,pu,tr_k} \quad (10)$$

where  $Q_{f,ij,initial}$  represents the value from the traditional power flow model and  $Q_{loss,ij}$  is the additional transformer branch reactive power loss due to a GMD. By explicitly including the additional reactive power losses due to GIC effects, the model upon which the state estimator is built is more accurate. By representing the nuances of the system during a GMD in the model, the estimator results will also be more accurate.

##### C. Changes in the Terms of the Jacobian Matrix

As the elements of the Jacobian matrix are essentially relating changes in measurement models with changes in the states, the addition of measurements and states in Section IV-A and models in Section IV-B necessarily leads to updates in the components of the WLS solution approach. The changes in the Jacobian matrix,  $\mathbf{H}$ , resulting from Eq. 4 belong to two categories. First, the new partial differentiation terms that represent the relationship between the reactive power flows and injections and the transformer neutral GIC system

states. Second, the additional partial differentiation terms that are added to the original terms relating reactive power flows and injections to the pu voltage magnitude states. These two modifications occur because the additional reactive power loss is modeled as dependent on the pu transformer neutral GIC and the pu voltage magnitude at the high side transformer bus.

Before examining the details of these terms, it is important to derive another expression - that of the partial differentiation of the pu effective GIC with respect to the pu neutral GIC for a given transformer. It can be derived as follows:

$$\begin{aligned} I_{eff, tr_k} &= |I_{h, tr_k} + I_{l, tr_k}/a_{tr_k}| \\ I_{eff, pu, tr_k} &= |I_{n, pu, tr_k} \times (r_{h, tr_k} + r_{l, tr_k}/a_{tr_k})| \\ \partial I_{eff, pu, tr_k} / \partial I_{n, pu, tr_k} &= \pm (r_{h, tr_k} + r_{l, tr_k}/a_{tr_k}) \end{aligned} \quad (11)$$

where,  $I_{eff, tr_k}$  is the effective GIC,  $I_{h, tr_k}$  is the high side GIC,  $I_{l, tr_k}$  is the low side GIC,  $I_{n, tr_k}$  is the neutral GIC,  $r_{h, tr_k}$  and  $r_{l, tr_k}$  are the ratios of high side and low side GICs respectively to the neutral GIC, and  $a_{tr_k}$  is the transformer turns ratio for transformer  $k$ . As the high and low side currents are not able to be realistically metered, the ratios of Eq. 11 are found as functions of the the available electric field information. Eq. 11 is a useful building block for obtaining the new GMD-related partial derivative terms.

1) *New partial differentiation terms in the Jacobian matrix:* The completely new terms of  $\mathbf{H}$  can be derived by partially differentiating Eqs. 9 and 10 by the pu neutral GIC at every transformer in the system. These terms are included as new columns relating the reactive power flows and injections affected by the transformer reactive power losses to the available neutral GIC measurements, hence, elongating the  $\mathbf{H}$  matrix horizontally. The terms are calculated using the following,

$$\frac{\partial Q_{inj, i}}{\partial I_{n, pu, tr_k}} = V_{pu, i} \times k_{pu, tr_k} \times \frac{\partial I_{eff, pu, tr_k}}{\partial I_{n, pu, tr_k}} \quad (12)$$

$$\frac{\partial Q_{f, ij}}{\partial I_{n, pu, tr_k}} = V_{pu, i} \times k_{pu, tr_k} \times \frac{\partial I_{eff, pu, tr_k}}{\partial I_{n, pu, tr_k}} \quad (13)$$

where  $V_{pu, i}$  is the pu voltage magnitude at the high side transformer bus,  $k_{pu, tr_k}$  is the scalar transformer parameter for transformer  $k$ , and  $\partial I_{eff, pu, tr_k} / \partial I_{n, pu, tr_k}$  is the partial differentiation term found by Eq. 11, and thus derivative of the electric field inputs.

2) *Additions to partial differentiation terms in the Jacobian matrix:* Changes to existing terms of  $\mathbf{H}$  can be derived by partially differentiating Eqs. 9 and 10 by the pu voltage magnitude at every transformer high side bus in the system. These terms are added to the already present terms which represent the sensitivity of the traditional reactive power flow and injection terms to the pu bus voltage. These additions do not have an effect on the Jacobian matrix dimensions. The terms are found using the following,

$$\frac{\partial Q_{inj, i}}{\partial V_{pu, i}} = \sum_{k=1}^{n_x} k_{pu, tr_k} \times I_{eff, pu, tr_k} \quad (14)$$

$$\frac{\partial Q_{f, ij}}{\partial V_{pu, i}} = k_{pu, tr_k} \times I_{eff, pu, tr_k} \quad (15)$$

where  $I_{eff, pu, tr_k}$  is the pu effective GIC per Eq. 11, determined from electric field data.

## D. Integration with State Estimation Methodology

Implementing these changes within the state estimation solution method outlined by Eqs. 7-8 involves the following. First, knowledge of the dc system parameters and system topology are used to extend the system model and state/measurement vectors. This information should be known because of the assessment required by NERC. If information is known about the expected error variance of the newly added GIC neutral measurements it is incorporated into the diagonal weight matrix  $\mathbf{R}$ . Then for every iteration  $k$ , electric field information, which may be measured or estimated and uniform or non-uniform, is used to estimate GIC ratios,  $r$ , and effective GICs which contribute to the calculation of  $\mathbf{H}(x^k)$ . Now, sufficient information is available to calculate the increment  $\Delta x^k$  of Eq. 7 and the next "best guess"  $x^{k+1}$ . This process is repeated until a maximum number of iterations or other stopping criterion is met.

## E. Bad Data Detection

Another important functionality of the state estimator is to detect and identify measurements with gross error, which can cause estimation interference. The largest normalized residual test is invoked to identify bad data in the proposed GIC-inclusive estimation framework [38], [39]. The residual can be found from the estimator solution  $\hat{\mathbf{x}}$  and is defined by  $\mathbf{r}(\hat{\mathbf{x}}) = \mathbf{z} - \mathbf{h}(\hat{\mathbf{x}})$ . The normalized residual for measurement  $i$  is calculated by

$$r_i^N(\hat{\mathbf{x}}) = \frac{r_i(\hat{\mathbf{x}})}{\sqrt{\Omega_{ii}(\hat{\mathbf{x}})}} \quad (16)$$

where the residual covariance matrix is defined by

$$\Omega(\hat{\mathbf{x}}) = \mathbf{R} - \mathbf{H}(\hat{\mathbf{x}})\mathbf{G}^{-1}(\hat{\mathbf{x}})\mathbf{H}^T(\hat{\mathbf{x}}). \quad (17)$$

If  $|r_{max}^N|$  is greater than a certain threshold, then there is reason to suspect the presence of data and the corresponding measurement could be eliminated from the measurement set and the states re-estimated. It should be noted that this method is not able to identify gross error in critical measurements; a more in-depth discourse on observability, critical measurements, and mitigating the effects of bad data on the state estimate is a subject for future work.

This section outlined the proposed changes to develop a GIC-inclusive state estimator, including augmentation of the state and measurement vectors, updates to the power flow and injection models, changes to elements within the Jacobian matrix used for solving the resulting WLS problem, and a bad data detection method. The following section describes the test cases used to validate the augmented estimation methods and the results that demonstrate improved accuracy during a GMD.

## V. RESULTS

The previously described method is implemented in MATLAB and makes use of the open-source products MATPOWER and MATGMD to enable some of the state estimation and GIC estimation functionality required. In this section, the inclusive estimator is applied to two cases under various GMD

conditions and is shown to provide more accurate results than GIC-agnostic methods during a GMD.

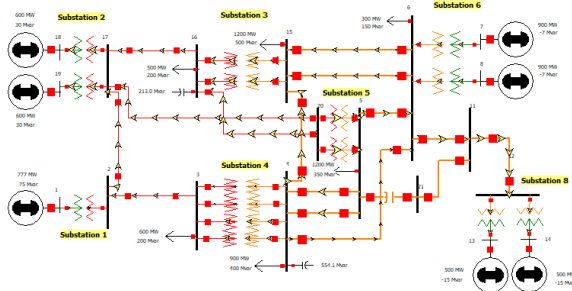


Fig. 2. One-line diagram of a 20-bus test case [24]

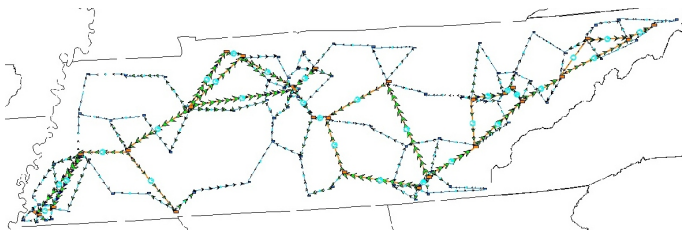


Fig. 3. One-line diagram for a synthetic 150 bus power system case. [25]

The GIC-inclusive state estimator was applied to a 500/345 kV 20 bus case in Fig. 2 and a 500/345 kV 150 bus system case in Fig. 3. GMD scenarios are simulated in commercially available power flow software and artificial noise added to the solution measurement values to emulate reality. The artificial noise added to the measurements follows a Gaussian distribution with standard deviations as follows: 0.01pu for power flows, 0.02pu for power injections, 0.01pu for node voltage magnitudes, and 0.001-0.005pu for neutral GICs. For the power flow measurements, the percentage of maximum measurements given as input ranged from 70%-85%. For the power injection measurements, the percentage of maximum measurements given as input range from 70%-95%. For the voltage magnitude measurements, the percentage of maximum measurements given as input is up to 80%. 50%-100% for neutral GICs. The true state solution is also retained for validation purposes. The electric field is assumed to be known with minimal error, for the purposes of determining current ratios and initializing estimation starting values. The representative results of the following GMD scenarios are presented:

- 1) Uniform electric field,
- 2) Non-uniform electric field,
- 3) Uniform electric field of fixed magnitude (4 V/km) and varying direction from  $0^\circ$  to  $180^\circ$ ,
- 4) Uniform electric field of increasing magnitude (1 V/km to 9 V/km) at a fixed direction ( $0^\circ$ ).

To quantify the accuracy of the proposed method, the difference between the known state values and the estimated states comprises a vector of errors.

Figs. 4 and 5 correspond to the 20 bus case affected by a uniform electric field and show the average absolute error (over 100 Monte Carlo simulations) in the voltage magnitude

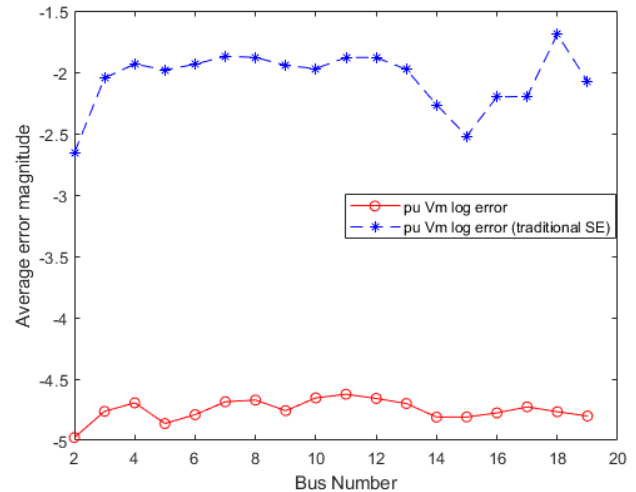


Fig. 4. Voltage magnitude decimal logarithmic absolute error for a uniform electric field on a 20 bus case

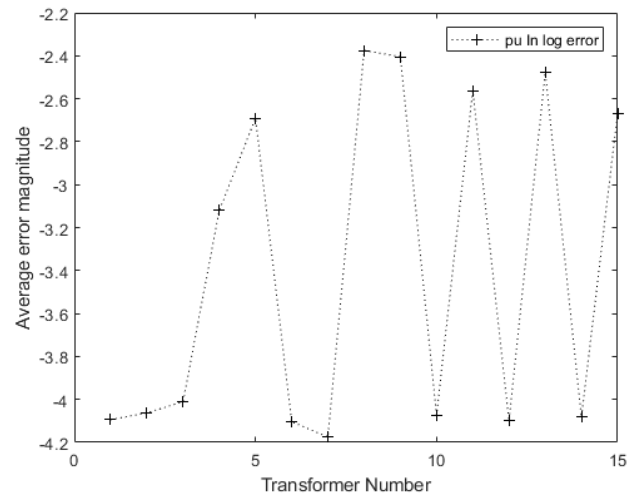


Fig. 5. Neutral GIC decimal logarithmic absolute error for a uniform electric field on a 20 bus system

and the neutral current state for the scenario where neutral GIC measurements are taken at random. The number of available measurements is kept at 50% of the total number of possible GIC measurements. The estimation error of the pu voltage magnitude state is in the range of  $10^{-5}$ , which is significantly less than that obtained by the traditional state estimator used during the GMD scenario, which is in the range of  $10^{-2}$ , if it even converges. Studies carried out in [22] indicated that the use of traditional state estimation during GMD situations may lead to non-convergence, which is an issue the GIC-inclusive state estimator did not face. Also, with around 50% neutral current measurements available, the error in the pu neutral GICs estimation, which is a parameter of interest in online GIC studies, is in the range of  $10^{-3}$ .

Figs. 6 and 7 correspond to the 20 bus case affected by a non-uniform electric field scenario. The plots show the average absolute error in the voltage magnitude and neutral current

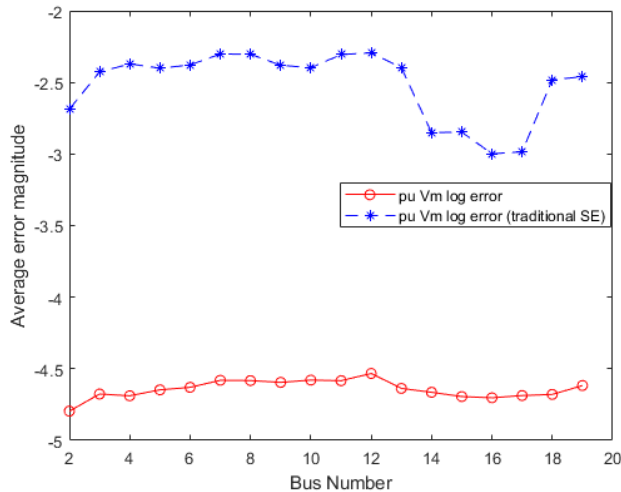


Fig. 6. Decimal logarithmic absolute error for the voltage magnitude state for a non-uniform electric field scenario on the 20 bus case

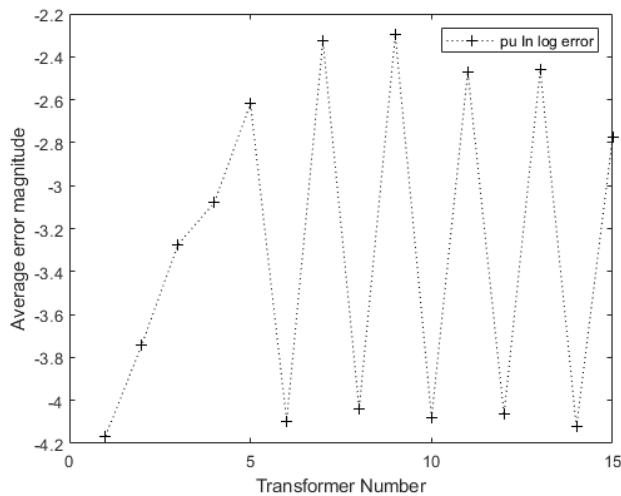


Fig. 7. Decimal logarithmic absolute error for the neutral GIC state for a non-uniform electric field scenario on the 20 bus case

states for a scenario where neutral GIC measurements are taken from only one transformer if many transformers with the same parameters are in parallel. The pu voltage magnitude estimation error is in the range of  $10^{-5}$ , which is much less than that obtained for the traditional state estimator which is in the range of  $10^{-2.5}$ . Again, this is only representative when the traditional state estimator even converges. With a current measurement available at one transformer from a set of parallel transformers, the pu neutral GIC state estimation error is in the range of  $10^{-3.2}$ . Fig. 8 depicts the estimation error profiles of the voltage magnitude (Vm) and neutral current (In) states at different uniform electric field directions ranging from 0 - 180° for a fixed magnitude. From the plot, it is clear that the error in the pu voltage magnitude states using GIC-inclusive estimation is lower than that of the traditional state estimator. The estimation error of neutral GICs is around  $10^{-4}$ . Fig. 9 depicts the estimation error profiles of

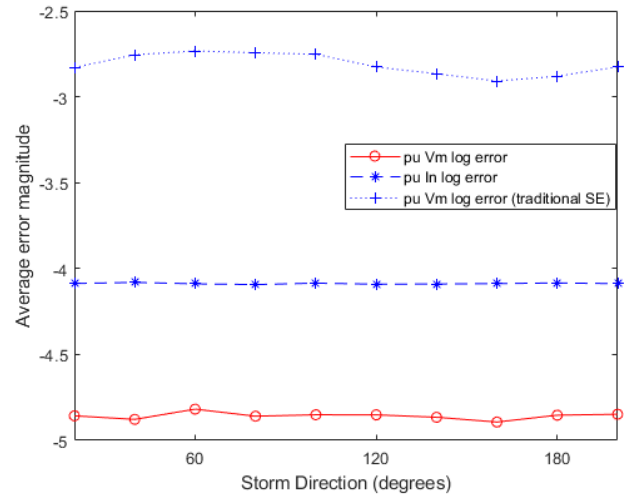


Fig. 8. Decimal logarithmic absolute error for the voltage magnitude and neutral GIC states along with the voltage magnitude state error from the traditional state estimator on a 150 bus case

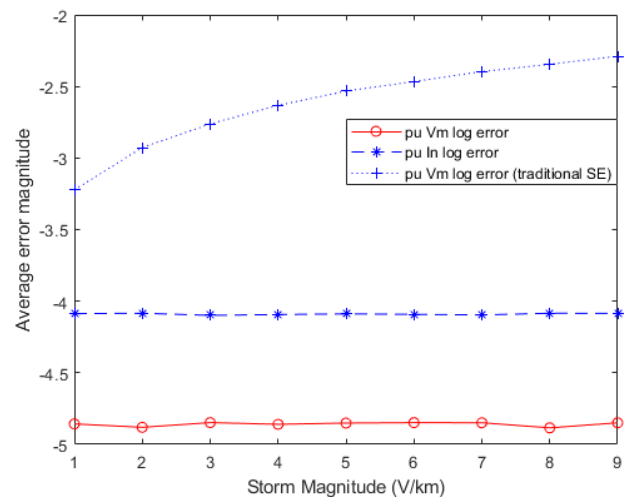


Fig. 9. Decimal logarithmic absolute error for the voltage magnitude and neutral GIC states along with the voltage magnitude state error from the traditional state estimator on a 150 bus case

the voltage magnitude and neutral current states at different uniform electric field magnitudes ranging from 1 - 9 V/km in a fixed direction. From the plot, it is clear that the error in the pu voltage magnitude states using GIC-inclusive estimation is lower than that of the traditional state estimator. The GIC-inclusive SE also has superior performance because all the scenarios carried out converged. With the traditional state estimator, especially with a larger case like the 150-bus case used here, the number of simulations that converge can be low. The estimation error of neutral GICs is around  $10^{-4}$ . The error pattern observed in the traditional state estimator (increasing error with increasing storm magnitude) is attributed to the fact that the lack of GMD-related modeling incurs increasing error as the GMD input increases. These patterns do not exist for the GIC-inclusive estimator error due to more accurate system modeling.

TABLE I  
AVERAGE ERROR WITH INCREASING ELECTRIC FIELD NOISE

Noise ( $\sigma$ )	Average Total Error
0.00	0.0090
0.01	0.0154
0.10	0.0996

Sensitivity to the number of available measurements incorporated is undertaken and shown in Fig. 10. When fewer than 50% of the transformer are metered, the estimator is prone to unobservability, but when the estimator converges the resulting estimate has acceptable accuracy. Sensitivity to the accuracy

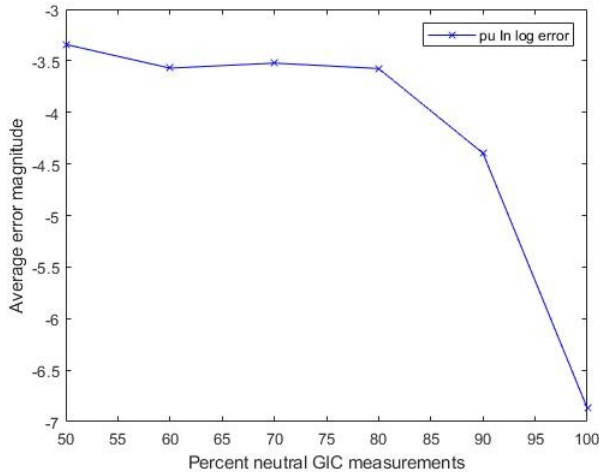


Fig. 10. Average error magnitude with increasing GIC measurement availability on a 150 bus case

of the electric field information is also explored. For a scenario on the 150 bus case with a non-uniform electric field, as the error of the electric field input increases, so does the resulting state estimation error, see Table I, but not prohibitively so. A scenario on the 150 bus case with a uniform electric field of 5V/km at 50° is graphically represented in Fig. 11. The increasing size of the dots show the increasing estimation error in neutral GIC states. The estimation error of the neutral GICs is mostly less than 0.05A. For this case, 70% of the neutral GICs and voltage magnitudes were available as measurements for the estimation process.

To determine the effectiveness of the proposed bad data detection methods, one of the measurements, chosen randomly by measurement type, is corrupted by  $4\sigma$ ,  $6\sigma$ , and  $10\sigma$ . Over hundreds of Monte Carlo simulation, the percentage of bad measurements correctly identified is plotted in Fig. 12. As important as it is that the method detects bad data correctly, it is also important that the test do not flag for bad data when there is none. The bad data detection false alarm rate when there is no egregiously bad data is 28.5%, 26.7%, and 29% for corrupted real power, reactive power, and voltage magnitude measurements, respectively. Future research into tuning the detection threshold could improve this metric.

With respect to computational efficiency, the GIC-inclusive state estimator takes as little as 2 seconds to solve the 150

bus system on an Intel Core i7-6500U @ 2.5 GHz. Time required per iteration for the GIC-inclusive state estimator is only around 0.5% more than that required by a traditional state estimator. For scenarios with a sizeable electric field applied, the conventional state estimator often fails to converge, but when it does it is in an average of 7 iterations. Meanwhile the GIC-inclusive state estimator was found to always converge in around 9 iterations with sufficient metering.

## VI. CONCLUSION

This paper addresses the improved implementation of PSSE during a GMD. It is found that inclusion of GIC-related states, measurements, and models is necessary to maintain estimation accuracy during abnormal conditions. The modeling of GICs is explained, along with the required changes to the traditional model. The results indicate that the GIC-inclusive state estimator accurately estimates the traditional and new GIC-related states in the presence of an underlying electric field. It helps overcome the issue of non-convergence that marred the traditional PSSE during a GMD. Therefore, utilities and system operators can greatly benefit from using this framework. Operator decision making during normal and abnormal operations depends on state estimation results and the system visibility during a large-scale GMD provided by the proposed methods could save the system from collapse. In addition to improving the estimation of existing states, the proposed modified estimator also provides important situational awareness for GIC-related values, namely neutral GICs.

Assumptions regarding system parameters, measurement availability, and measurement accuracy were made in this initial implementation. Future work will address these topics. Additional analysis in the physical world is necessary to improve parameter modeling; the modular nature of the proposed estimation framework enables convenient updating of the dc system information as it becomes available. The addition of neutral current states requires additional measurements to maintain observability, a complex but well-understood topic with respect to traditional estimation. Research into the dependencies between the new states and measurements could provide valuable insight for future iterations of GIC-inclusive estimators. These relationships may ultimately help obtain the conditions for critical measurements and lay the groundwork for GIC-inclusive estimation bad data detection. Reliable electric field measurements or estimates for the given GMD scenario are a useful input to the GIC-inclusive ac state estimator. A dc GIC estimator could obtain fairly accurate electric field estimates from magnetic field, transformer, and earth data. A sequential combination of these estimators could be especially effective, using the dc estimator output to generate additional measurements, or pseudomeasurements, for the ac estimator. In practice, this may make the best use of available measurements to maintain observability and improve accuracy. Regarding measurement accuracy, the standard estimator relies on an assumed model of measurement noise. An appropriate noise model for GIC-related values is an area for future research. It would also be of interest to consider how the estimate error changes for different and possibly wrong error

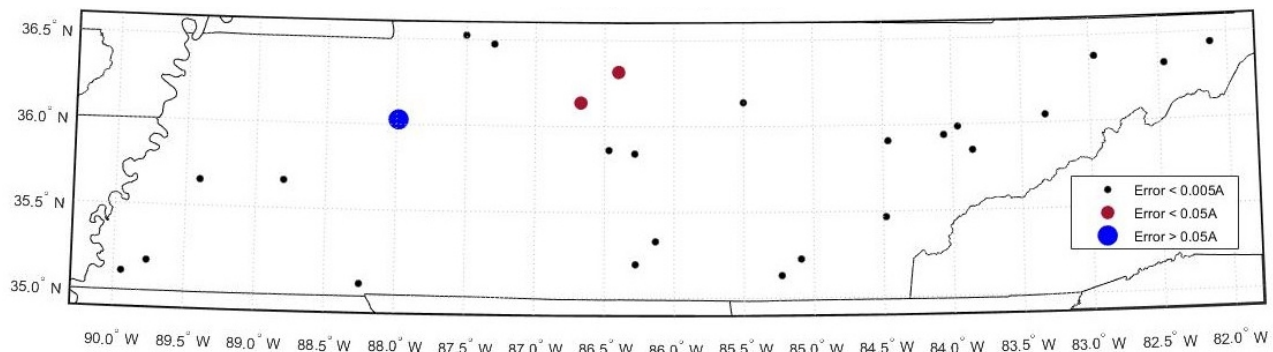


Fig. 11. Geographical representation of error magnitude in neutral GIC estimates for a 150-bus case set on the footprint of Tennessee

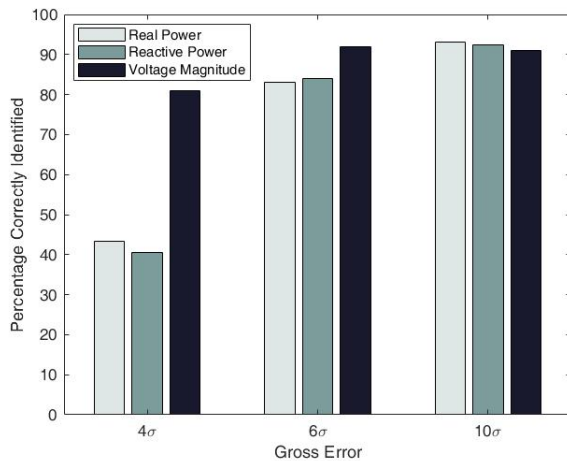


Fig. 12. Percentage of bad data instances correctly identified as a function of the data badness

models. Understanding the error model directly informs the weighting factors used in the estimation algorithm.

The proposed GIC-inclusive ac state estimator provides extended system states with sufficient accuracy during GMD events. This ability is dependent on factors for future work such as system parameters, availability and placement of measurements, and the use of a dc state estimator to provide pseudomeasurements, but overall an improved model and method are proposed for PSSE during a GMD.

## REFERENCES

- [1] "High-Impact, Low-Frequency Event Risk to the North American Bulk Power System," North American Electric Reliability Corporation (NERC), Tech. Rep., June 2009.
- [2] J. Kappenman, "A Perfect Storm of Planetary Proportions," *IEEE Spectrum*, vol. 49, no. 2, 2012.
- [3] V. D. Albertson, J. M. Thorson, R. E. Clayton, and S. C. Tripathy, "Solar-Induced-Currents in Power Systems: Cause and Effects," *IEEE Transactions on Power Apparatus and Systems*, vol. PAS-92, no. 2, pp. 471–477, March 1973.
- [4] "March 13, 1989 Geomagnetic Disturbance," North American Electric Reliability Corporation (NERC), Tech. Rep., Aug 1990.
- [5] P. Czech, S. Chano, H. Huynh, and A. Dutil, "The Hydro-Quebec System Blackout of 13 March 1989: System Response to Geomagnetic Disturbance," in *Proc. EPRI Conf. Geomagnetically Induced Currents*, 1992.
- [6] "Transmission System Planned Performance for Geomagnetic Disturbance Events NERC Std. TPL-007-1," North American Electric Reliability Corporation (NERC), Tech. Rep., June 2014.
- [7] "Transmission System Planned Performance for Geomagnetic Disturbance Events NERC Std. TPL-007-2," North American Electric Reliability Corporation (NERC), Tech. Rep., October 2017.
- [8] J. Berge, L. Marti, and R. K. Varma, "Modeling and mitigation of Geomagnetically Induced Currents on a realistic power system network," in *2011 IEEE Electrical Power and Energy Conference*, Oct 2011, pp. 485–490.
- [9] M. Kazerooni, H. Zhu, T. J. Overbye, and D. A. Wojtczak, "Transmission System Geomagnetically Induced Current Model Validation," *IEEE Transactions on Power Systems*, vol. 32, no. 3, pp. 2183–2192, 2017.
- [10] A. A. Trichtchenko, D. H. Boteler, and A. Foss, "GIC Modelling for an Overdetermined System," in *Canadian Conference on Electrical and Computer Engineering, 2006. CCECE'06*. IEEE, 2006, pp. 394–397.
- [11] B. Kovan and F. De Leon, "Mitigation of Geomagnetically Induced Currents by Neutral Switching," *IEEE Transactions on Power Delivery*, vol. 30, no. 4, pp. 1999–2006, 2015.
- [12] D. Boteler and R. Pirjola, "Comparison of Methods for Modelling Geomagnetically Induced Currents," in *Annales Geophysicae*, vol. 32, no. 9. Copernicus GmbH, 2014, pp. 1177–1187.
- [13] T. J. Overbye, T. R. Hutchins, K. Shetye, J. Weber, and S. Dahman, "Integration of Geomagnetic Disturbance Modeling into the Power Flow: A Methodology for Large-Scale System Studies," in *North American Power Symposium (NAPS), 2012*. IEEE, 2012, pp. 1–7.
- [14] F. C. Schweppe, "Power System Static-State Estimation, Part III: Implementation," *IEEE Transactions on Power Apparatus and Systems*, vol. PAS-89, no. 1, pp. 130–135, Jan 1970.
- [15] A. Abur and A. Gomez, *Power System State Estimation-Theory and Implementations*. Marcel Dekker, Inc., 2004.
- [16] A. Monticelli, "Electric Power System State Estimation," *Proceedings of the IEEE*, vol. 88, no. 2, pp. 262–282, Feb 2000.
- [17] S. Soltan, M. Yannakakis, and G. Zussman, "Power grid state estimation following a joint cyber and physical attack," *IEEE Transactions on Control of Network Systems*, vol. 5, no. 1, pp. 499–512, March 2018.
- [18] J. Zhao, L. Mili, and A. Abdelhadi, "Robust dynamic state estimator to outliers and cyber attacks," in *2017 IEEE Power Energy Society General Meeting*, July 2017, pp. 1–5.
- [19] C. Gonzalez-Perez and B. F. Wollenberg, "Analysis of massive measurement loss in large-scale power system state estimation," *IEEE Transactions on Power Systems*, vol. 16, no. 4, pp. 825–832, Nov 2001.
- [20] B. F. Woollenberg, "Power system state estimators: designed for reliability or accuracy?" in *2004 International Conference on Probabilistic Methods Applied to Power Systems*, Sep. 2004, pp. 618–621.
- [21] J. Xie, A. P. S. Meliopoulos, B. Xie, C. Zhong, and K. Liu, "Gеоelectric field estimation during geomagnetic disturbances," in *2019 IEEE Power Energy Society General Meeting (PESGM)*, Aug 2019, pp. 1–5.
- [22] C. Klauber, G. P. Juvekar, K. Davis, T. J. Overbye, and K. Shetye, "The Potential for a GIC-inclusive State Estimator," in *2018 North American Power Symposium (NAPS)*, Sep. 2018, pp. 1–6.
- [23] R. D. Zimmerman, C. E. Murillo-Sanchez, and R. J. Thomas, "MAT-POWER: Steady-State Operations, Planning, and Analysis Tools for Power Systems Research and Education," *IEEE Transactions on Power Systems*, vol. 26, no. 1, pp. 12–19, Feb 2011.
- [24] R. Horton, D. Boteler, T. J. Overbye, R. Pirjola, and R. C. Dugan, "A test case for the calculation of geomagnetically induced currents," *IEEE*



- Transactions on Power Delivery*, vol. 27, no. 4, pp. 2368–2373, Oct 2012.
- [25] A. B. Birchfield, T. Xu, K. M. Gegner, K. S. Shetye, and T. J. Overbye, “Grid structural characteristics as validation criteria for synthetic networks,” *IEEE Transactions on Power Systems*, vol. 32, no. 4, pp. 3258–3265, 2017.
- [26] D. H. Boteler and R. J. Pirjola, “Modelling Geomagnetically Induced Currents Produced by Realistic and Uniform Electric Fields,” *IEEE Transactions on Power Delivery*, vol. 13, no. 4, pp. 1303–1308, Oct 1998.
- [27] J. Kappenman, V. Albertson, and N. Mohan, “Investigation of Geomagnetically Induced Currents in the Proposed Winnipeg-Duluth-Twin Cities 500-kV Transmission Line,” *NASA STI/Recon Technical Report N*, vol. 82, 1981.
- [28] A. Viljanen, “Relation of Geomagnetically Induced Currents and Local Geomagnetic Variations,” *IEEE Transactions on Power Delivery*, vol. 13, no. 4, pp. 1285–1290, 1998.
- [29] V. D. Albertson, J. G. Kappenman, N. Mohan, and G. A. Skarbakka, “Load-Flow Studies in the Presence of Geomagnetically-Induced Currents,” *IEEE Transactions on Power Apparatus and Systems*, vol. PAS-100, no. 2, pp. 594–607, Feb 1981.
- [30] T. J. Overbye, K. S. Shetye, T. R. Hutchins, Q. Qiu, and J. D. Weber, “Power Grid Sensitivity Analysis of Geomagnetically Induced Currents,” *IEEE Transactions on Power Systems*, vol. 28, no. 4, pp. 4821–4828, Nov 2013.
- [31] R. A. Walling and A. N. Khan, “Characteristics of transformer exciting-current during geomagnetic disturbances,” *IEEE Transactions on Power Delivery*, vol. 6, no. 4, pp. 1707–1714, 1991.
- [32] Xuzhu Dong, Yilu Liu, and J. G. Kappenman, “Comparative analysis of exciting current harmonics and reactive power consumption from gic saturated transformers,” in *2001 IEEE Power Engineering Society Winter Meeting. Conference Proceedings (Cat. No.01CH37194)*, vol. 1, 2001, pp. 318–322 vol.1.
- [33] X. Dong, Y. Liu, and J. G. Kappenman, “Comparative Analysis of Exciting Current Harmonics and Reactive Power Consumption from GIC Saturated Transformers,” in *2001 IEEE Power Engineering Society Winter Meeting. Conference Proceedings (Cat. No. 01CH37194)*, vol. 1, Jan 2001, pp. 318–322 vol.1.
- [34] A. Rezaei-Zare, “Reactive power loss versus gic characteristic of single-phase transformers,” *IEEE Transactions on Power Delivery*, vol. 30, no. 3, pp. 1639–1640, 2015.
- [35] Space Weather Prediction Center, National Oceanic and Atmospheric Administration (NOAA), “Geoelectric field 1-minute.” [Online]. Available: <https://www.swpc.noaa.gov/products/geoelectric-field-1-minute>
- [36] C. Klauber, K. Shetye, T. Overbye, and K. Davis, “A GIC Estimator for Electric Grid Monitoring During Geomagnetic Disturbances,” *IEEE Transactions on Power Systems*, pp. 1–1, 2020.
- [37] G. P. Juvekar and K. Davis, “MATGMD: A Tool for Enabling GMD Studies in MATLAB,” in *2019 IEEE Texas Power and Energy Conference (TPEC)*, Feb 2019, pp. 1–6.
- [38] E. Handschin, F. C. Schweppe, J. Kohlas, and A. Fiechter, “Bad data analysis for power system state estimation,” *IEEE Transactions on Power Apparatus and Systems*, vol. 94, no. 2, pp. 329–337, 1975.
- [39] T. V. Cutsem, M. Ribbens-Pavella, and L. Mili, “Bad Data Identification Methods In Power System State Estimation-A Comparative Study,” *IEEE Transactions on Power Apparatus and Systems*, vol. PAS-104, no. 11, pp. 3037–3049, 1985.
- Gandhali Prakash Juvekar** (S’18) received the B.Tech degree in electrical and electronics engineering from National Institute of Technology, Surathkal, Karnataka, India in 2017 and the M.S. degree in electrical engineering from the Texas A&M University (TAMU), College Station, TX, USA in 2019. Her research interests include protective relaying and GMD analysis.
- Cecilia Klauber** (S’12) received the B.S. degree in electrical engineering from Baylor University, Waco, TX, USA in 2014 and the M.S. degree in electrical engineering from the University of Illinois at Urbana-Champaign, Champaign, IL, USA. She is currently a Ph.D student in electrical engineering at Texas A&M University, College Station, TX, USA. Her research interests include power system monitoring and geomagnetic disturbance analysis.
- Dr. Katherine R. Davis** (S’05-M’12-SM’18) received the B.S. degree from the University of Texas at Austin, Austin, TX, USA, in 2007, and the M.S. and Ph.D. degrees from the University of Illinois at Urbana-Champaign (UIUC), Urbana, IL, USA, in 2009 and 2011, respectively, all in electrical engineering. She is currently an Assistant Professor in electrical and computer engineering with Texas A&M University, College Station, TX, USA.
- Dr. Thomas J. Overbye** (S’87-M’92-SM’96-F’05) received B.S., M.S., and Ph.D. degrees in electrical engineering from the University of Wisconsin Madison, Madison, WI, USA. He is currently with Texas A&M University where he is a Professor and holder of the Erle Nye ‘59 Chair for Engineering Excellence.
- Komal Shetye** (S’10-M’11-SM’18) received the B. Tech and MSEE degrees in electrical engineering from the University of Mumbai, India and the University of Illinois at Urbana-Champaign, IL, USA, in 2009 and 2011, respectively. She is currently an Associate Research Engineer with the Texas Engineering Experiment Station (TEES) and the Department of Electrical Engineering, Texas A&M University, College Station, TX, USA.